ADVANCED FUNCTIONAL MATERIALS
www.afm-journal.de

Toward Flexible Spintronics: Perpendicularly Magnetized Synthetic Antiferromagnetic Thin Films and Nanowires on Polyimide Substrates

T. Vemulkar, R. Mansell, A. Fernández-Pacheco, and R. P. Cowburn*

The successful fabrication of ultra-thin films of CoFeB/Pt with strong perpendicular magnetic anisotropy and antiferromagnetic interfacial interlayer coupling on flexible polyimide substrates is demonstrated. Despite an increased surface roughness and defect density on the polyimide substrate, magnetic single layers of CoFeB still show sharp coercive switching. Magnetic Kerr imaging shows that the magnetization reversal is dominated by a greater density of nucleation sites than the identical film grown on Si. These layers maintain their magnetic characteristics down to a radius of curvature of 350 ± µm. Further, antiferromagnetically (AF) Ruderman-Kittel-Kasuya-Yoshida (RKKY) coupled bilayers of CoFeB were fabricated which are robust under bending and the coupling strength is successfully modulated via interlayer engineering. Finally, a perpendicular synthetic antiferromagnetic (SAF) thin film grown on a polyimide substrate is patterned into straight 10 µm long nanowires down to 210 nm in width that displayed the robust switching characteristics of the thin film. These are extremely promising results for the fabrication of robust, flexible, magneto-electronic, non-volatile memory, logic, and sensor devices.

Recent progress in the fabrication of electronic systems on flexible substrates has led to research in applications ranging from electronic skins to bendable light emitting screens.[1–3] However, it is still a significant challenge and an active area of research to fabricate flexible, nonvolatile memory elements, and recent work has been focused primarily on memory devices based on field effect transistor systems.[4–6] An alternative, technologically relevant solution is to use devices based on magnetic materials.

Flexible magnetoelectronic devices to date have generally been focused on sensors using giant magnetoresistance (GMR) elements with in-plane magnetized layers[7,8] and improving GMR performance on flexible substrates is of technological interest.[9,10] However, perpendicular magnetic anisotropy (PMA) materials are generally of greater relevance with regards to nonvolatile memory applications and magnetic field sensors. A particular challenge arises in fabricating PMA multilayer based magnetoelectronic devices on flexible substrates since the quality of the interface between the various layers, which is often strongly dependent on the device substrate and buffer layers used, can significantly alter key characteristics of these magnetic thin film heterostructures such as the magnitude of the PMA[11,12] and interlayer exchange coupling effects.[12,13] Further, the thickness of the magnetic layers in PMA multilayer stacks are often in the sub-nanometer range. Hence, producing these devices on flexible substrates is a significant challenge due to substrate roughness and defect density considerations. It is therefore remarkable that we have fabricated thin films and nanowires with both strong PMA as well as tunable interlayer exchange coupling effects on a polyimide substrate, and is a first step toward flexible PMA based magnetoelectronic devices.

PMA based multilayer thin films are extremely interesting from the perspective of fundamental physics, as well as commercial memory and logic applications. Perpendicular magnetic tunnel junctions (p-MTJs) fabricated from multilayer heterostructures of perpendicularly magnetized thin films are a prime candidate for tunneling magnetoresistance (TMR) based magnetic random access memory (MRAM)—the next generation of non-volatile memory devices.[14] They offer bit scalability and thermal stability down to sub-20 nm due to their strong PMA, and a low switching current due to their high spin transfer torque efficiency.[15,16] Spin orbit interaction effects in such PMA multilayer heterostructures also offer the potential of fabricating ultralow power memory and logic devices[17–19] and can drive the motion[20] of characteristically narrow and fast moving domain walls.[21] Hence, they are also attractive for a variety of current induced domain wall motion (CIDWM) based magnetic memory and logic elements,[22] most notably enabling significant progress in racetrack memory architectures.[17,23]

Further, PMA materials in conjunction with antiferromagnetic (AF) coupling are of significant technological relevance for MRAMs using spin transfer torque (STT) switching,[24,25] as well as sensors[26,27] and novel 3D logic applications.[28] Perpendicular synthetic antiferromagnetic (SAF) nanowires in particular are of great scientific interest and have recently been

T. Vemulkar, Dr. R. Mansell, Dr. A. Fernández-Pacheco, Prof. R. P. Cowburn
Cavendish Laboratory
University of Cambridge
JJ Thomson Avenue, Cambridge CB3 0HE, UK
E-mail: tv243@cam.ac.uk

DOI: 10.1002/adfm.201505138

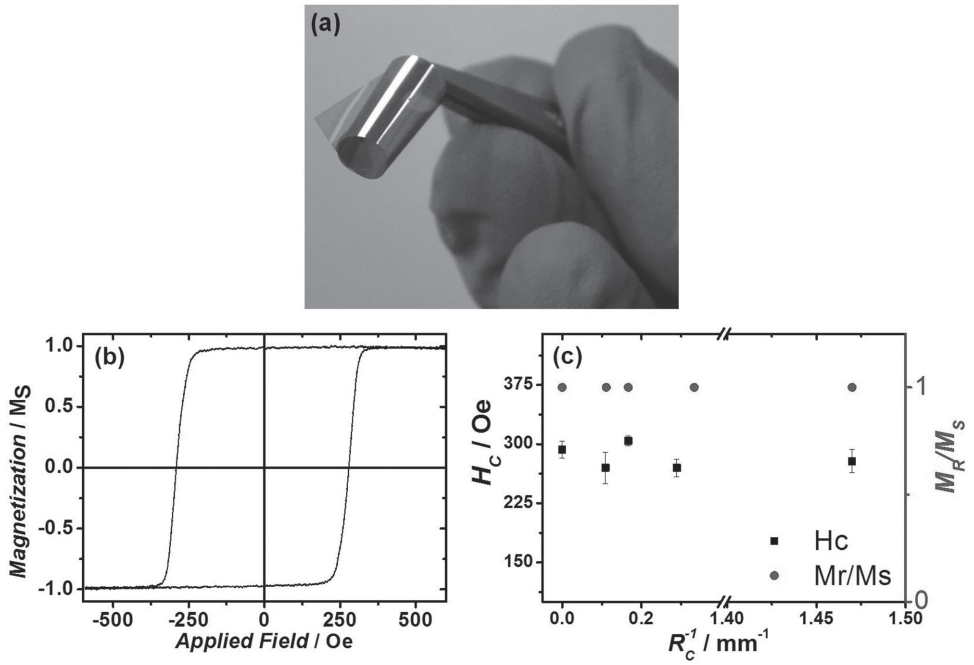

Figure 1. a) A perpendicular magnetic multilayer thin film fabricated on a flexible polyimide substrate. b) The polar magneto-optical Kerr effect (MOKE) loop of a single layer of 0.8 nm thick CoFeB grown on a polyimide substrate. c) The remanent magnetization and coercivity as a function of bending radius for the film in (b).

shown to have enabled a fundamental development in domain wall based memory systems.[29] Finally, TMR based MTJs find applicability not only in memory applications, but are also of relevance for high sensitivity magnetic field sensor devices.[30] We show here the fabrication of perpendicular CoFeB ultrathin films on flexible polyimide substrates. We also successfully fabricate tunable, perpendicular SAF thin films via antiferromagnetic Ruderman–Kittel–Kasuya–Yosida (RKKY) interlayer coupling of CoFeB bilayers on flexible polyimide substrates. We further pattern a perpendicular SAF thin film into nanowires with widths down to 210 nm that maintain the magnetic characteristics of the thin film. The nanopatterned perpendicular multilayer heterostructures with tunable exchange coupling effects on flexible substrates fabricated in this work may open the way for new flexible sensors, magnetic memory elements, and even new flexible spintronic devices.

Figure 1a shows a perpendicular CoFeB/Pt thin film on a flexible polyimide substrate. A representative polar magneto-optical Kerr effect (MOKE) magnetic hysteresis loop of a thin film of Ta(4)/Pt(6)/CoFeB(0.8)/Pt(2) with thicknesses in nm when grown on flat polyimide is shown in Figure 1b, and Figure 1c summarizes the remanent magnetization and coercivity of such a film when bent over a range of different radii. The thin film retains its full remanent magnetization and coercivity under bending, and these characteristics are robust down to a radius of bending far less than the ≈1 cm bending radius of most envisioned flexible electronics applications.[31]

Figure 2 compares the magnetic properties of single CoFeB layers of increasing thickness on Si, flat polyimide, and bent polyimide with a radius of curvature (R_C) of 350 ± 50 µm. The magnetic multilayer stack used here is Ta(4)/Pt(6)/CoFeB(0.7-1.2)/Pt(2) with thicknesses in nm. Figure 2a shows that films fabricated on polyimide substrates generally displayed slightly lower anisotropy for the same CoFeB thickness due to the poorer substrate conditions.[32] We observe the expected $1/t$ dependence of anisotropy with increasing CoFeB thickness[33] on both the Si and polyimide substrate as measured by the hard axis saturation field H_K.[34] The decreasing PMA with increasing CoFeB thickness is because PMA is an interfacial effect that is dominant in ultrathin CoFeB/Pt multilayers. The total magnetic anisotropy can be separated into an interfacial contribution and a volume contribution. As the thickness of the magnetic layer is increased, it approaches the spin reorientation transition. At this point the magnetization direction will be dominated by the volume contribution to the magnetic anisotropy which arises from long range dipolar interactions in the thin film and is described by a demagnetizing field. This is known as the shape anisotropy effect, and it favors a magnetization orientation in the plane of the film. This decreasing trend in anisotropy is accompanied by a decrease in the coercivity as seen in Figure 2b since it becomes easier to nucleate a domain of contrary magnetization direction with decreasing anisotropy.

Figure 2c–h shows the polar MOKE hysteresis loops of perpendicular single layers of CoFeB on substrates of Si, flat polyimide, and bent polyimide with a R_C of 350 ± 50 µm. The magnetization reversal process between the two substrates is notably different. The CoFeB single layers on the Si substrates display rectangular hysteresis loops with sharp magnetic switching as seen in Figure 2c–h (black curves) which is evidence of domain wall motion dominated magnetic reversal. This type of magnetic reversal process in PMA CoFeB is dominated by the nucleation of large, roughly circular domains with domain walls that rapidly expand through the thin film.[35] **Figure 3**a shows the expansion of one such domain that was imaged during the

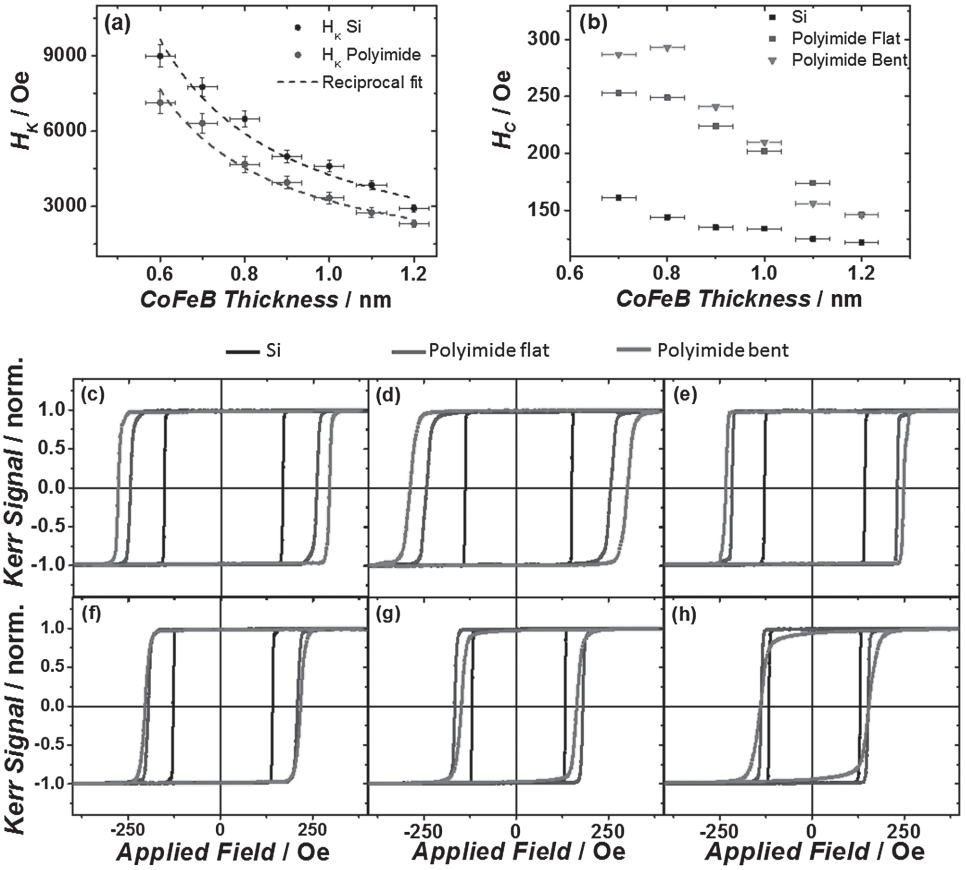

Figure 2. a) The hard axis saturation field versus CoFeB thickness for Si and flat polyimide substrates. b) The coercive field versus CoFeB thickness for Si, a flat polyimide substrate, and a bent polyimide substrate with a radius of curvature (R_C) of 350 ± 50 µm. c–h) Polar MOKE hysteresis loops at a field rate of 1000 Oe s^{-1} of single CoFeB layers on Si, a flat polyimide substrate, a bent polyimide substrate with a R_C of 350 ± 50 µm. Layer thicknesses are (c) 0.7 nm, (d) 0.8 nm, (e) 0.9 nm, (f) 1.0 nm, (g) 1.1 nm, and (h) 1.2 nm.

magnetic reversal of a 0.8 nm film of CoFeB and demonstrates this reversal mechanism. This sharp magnetic switching is expected on the Si substrate, due to a low inherent root mean square (RMS) roughness of 0.431 nm that was measured in a 7×7 µm^2 area in Figure 3c which was masked to minimize the contribution of point defects to the RMS roughness, as well as an extremely low defect population as seen in the atomic force microscopy (AFM) scan in Figure 3c.

We next study the reversal process on the polyimide substrate. We notice quite square loops with robust magnetic switching despite the increased roughness of the polyimide substrate which is extremely promising for device characteristics. In considering the polar MOKE loops on the polyimide substrate in Figure 2c–f, we observe a significantly increased coercivity compared to the Si substrate. We attribute the increased coercivity to increased domain wall pinning due to the presence of a higher defect density in the form of peaks and pits, on the scale of tens and hundreds of nanometers in width and height as seen on the AFM scan in Figure 3d. These defects can act to pin or trap domain walls due to local changes in anisotropy or film thickness.[36–38] This is further evidenced by the domain imaging of a 0.8 nm CoFeB layer on the polyimide substrate in Figure 3b where we observe significant domain wall pinning and a larger number of nucleation sites than Figure 3a.

Figure 2g,h corresponds to 1.1 and 1.2 nm thick layers of CoFeB. The decreased anisotropy closer to the spin reorientation transition in these films both leads to a higher number of reversal domains, and effectively reduces the anisotropy difference around defects that act to trap domain walls. These effects reduce the coercivity because the domain wall pinning effect is now less pronounced, and the coercive field (H_C) on polyimide approaches those of the identical film grown on Si.

The buffer layers in magnetic multilayer thin films are often crucial to obtaining robust PMA. This is especially true on the polyimide substrate here, where the substrate conditions are inherently poor as evidenced by a RMS roughness of 2.8 nm. This was measured from a 7×7 µm^2 area in Figure 3d masked specifically to minimize the contribution of large point defects to the RMS roughness value. We characterize the roughness profile of the polyimide substrate further in supplementary Figure 3. We illustrate how the buffer layers reduce the amplitude specifically of high frequency, short wavelength spatial undulations on the bare polyimide substrate that have a cut-off wavelength of ≈20 nm or less. The reduction in the RMS roughness in this wavelength range is significant, from 0.440 nm on a bare polyimide substrate, to 0.232 nm on a Ta(4)/Pt(6)/CoFeB(0.7)/Pt(2) magnetic thin film (thicknesses in nm) that was grown on a polyimide substrate. The cut-off wavelength is comparable to

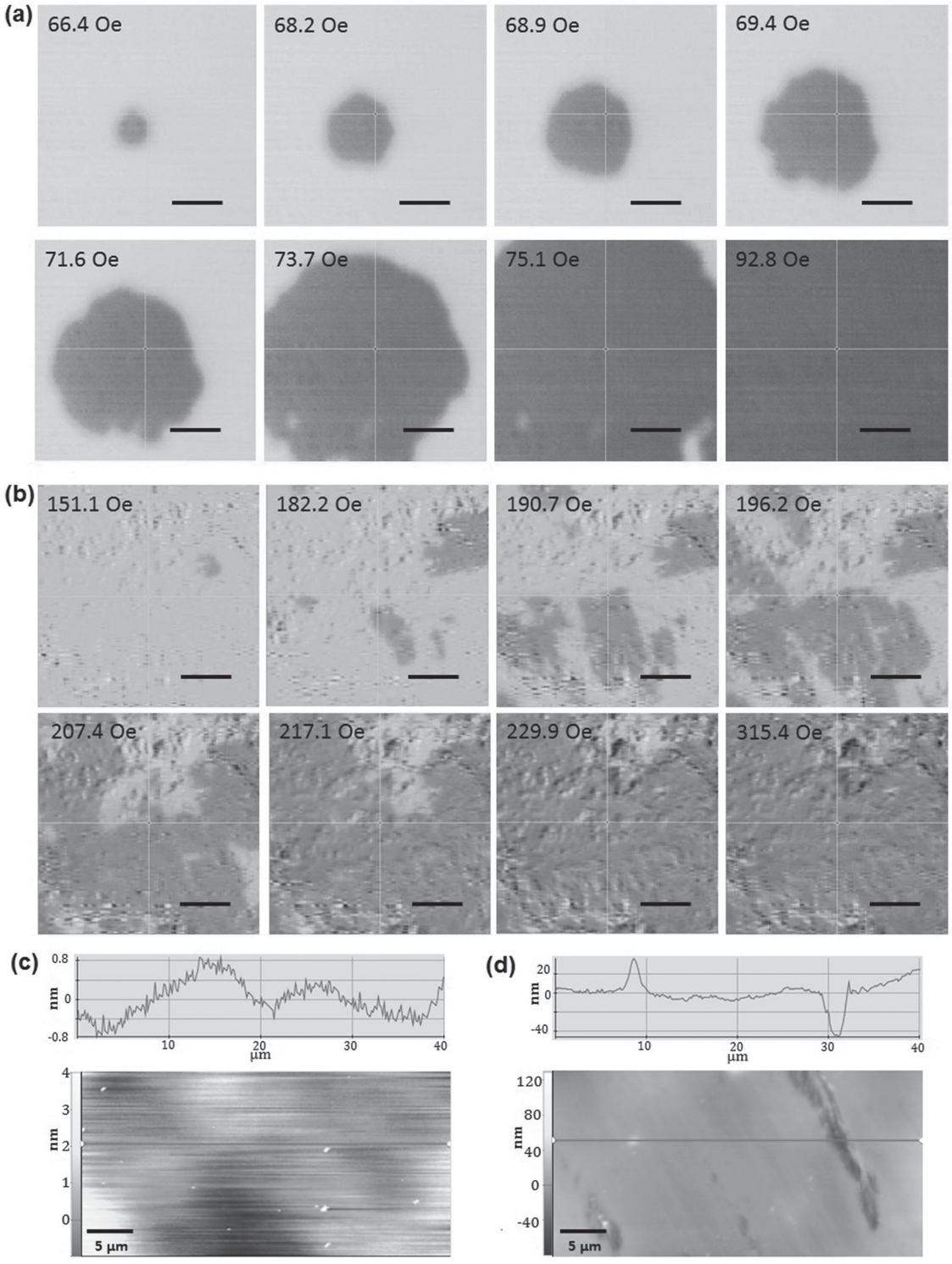

Figure 3. Kerr microscopy images showing domain nucleation and expansion processes for 0.8 nm CoFeB films in a pulsed field grown on a) Si and b) polyimide substrates. All scale bars for the domain images correspond to 100 µm. c,d) The substrate AFM scans corresponding to (a) and (b), respectively. Note the difference in scale between (c) and (d).

the ≈10 nm domain wall widths typically observed in such PMA materials systems.[21] Hence a reduction in the roughness at this spatial length scale is expected to have a significant effect on the nucleation and pinning of magnetic domain walls during the magnetic reversal process.[39] We evidence this in supplementary **Figure 4**, where we demonstrate how significantly the magnetic properties are affected by the smoothing effect of the Ta layer,[40,41] highlighting the role of the buffer in promoting PMA

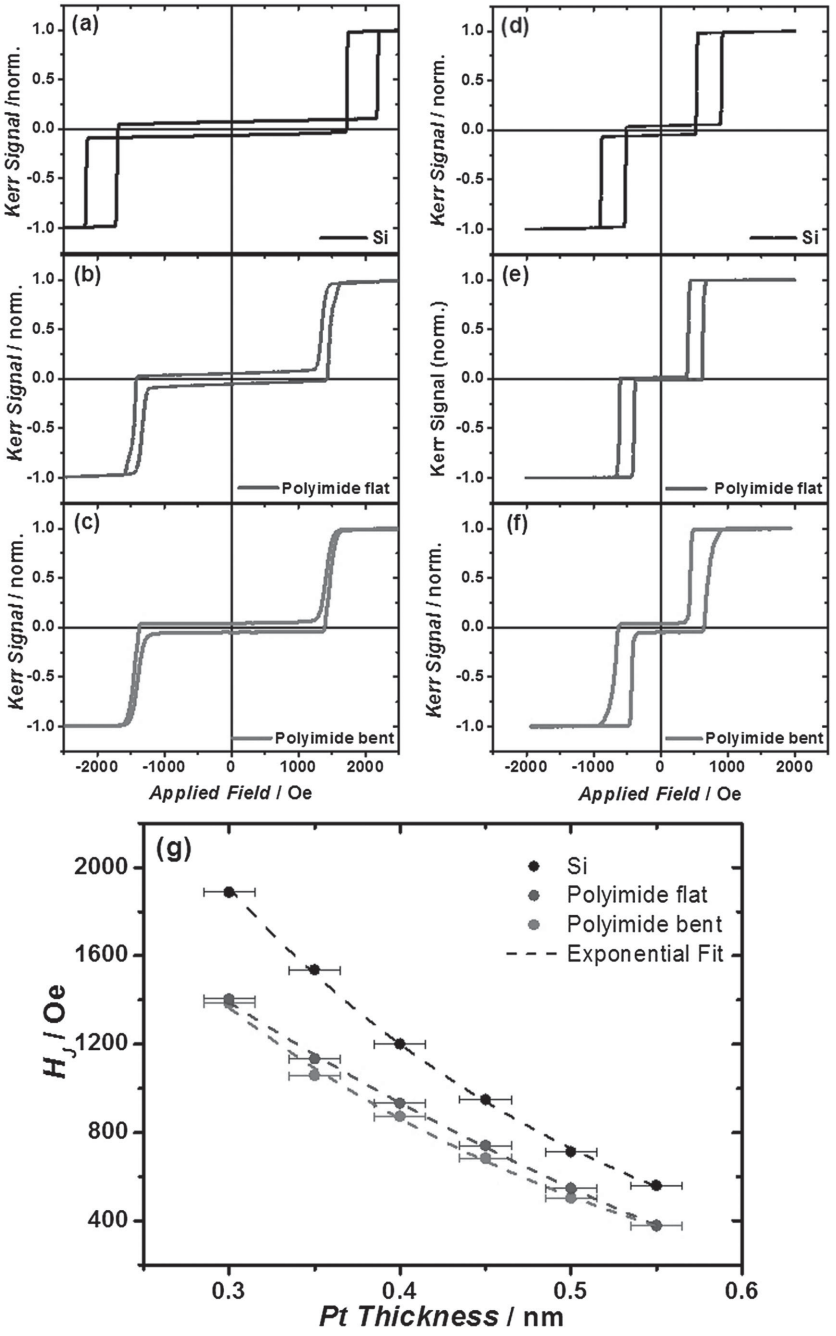

Figure 4. Polar MOKE loops of RKKY coupled bilayers with Pt interlayer thickness of 0.3 nm on a) Si, b) at polyimide and c) bent polyimide with a R_C of 350 ± 50 μm, and Pt interlayer thickness of 0.5 nm on d) Si, e) at polyimide and f) bent polyimide with a R_C of 350 ± 50 μm. g) The magnitude of the RKKY coupling field as a function of Pt interlayer thickness for each substrate.

in thin films especially when using rough initial conditions as is expected on most flexible substrates.

The robust magnetic characteristics are maintained under bending the polyimide substrates to a R_C of 350 ± 50 μm. This is clearly evidenced by the red curves in Figure 2c–h. Slight differences in the shape and coercivity of the transitions between the flat and bent polyimide is attributed to the local topography around the MOKE laser spot which has a significant effect on the magnetization reversal process.

Having characterized the key properties of CoFeB single layers on polyimide substrates, we further successfully demonstrate RKKY coupled bilayers on a similar polyimide substrate, and compare the RKKY coupling to that of the identical bilayers grown on Si substrates. The RKKY coupled bilayer stack used here is Ta(2)/Pt(3)/CoFeB(0.8)/Pt(t)/Ru(0.9)/Pt(t)/ CoFeB(0.8)/Pt(2) with thicknesses in nm. The thickness of the Ru was chosen to lie at the first AF coupling peak[42] and the Ta/Pt buffer for this stack was optimized to maximize the RKKY

coupling magnitude and is shown in supplementary **Figure 5**. The Pt layers on either side of the Ru layer stabilize the PMA and can be used to exponentially increase the magnitude of the RKKY coupling by decreasing their thickness.[43] We successfully demonstrate this tuning of the magnitude of the RKKY coupling on a flexible polyimide substrate, even under bending. We note that for films grown on the polyimide substrate the thickness of the Pt layers on either side of the Ru coupling layer has a more significant effect on the magnetic reversal than for the stacks grown on Si. At lower Pt thicknesses (Figure 4a–c), we observe more slanted transitions with low coercivities on the polyimide. This is attributed to the reduced perpendicular anisotropy due to the relatively thin Pt interlayers on either side of the Ru that are less able to stabilize the magnetic anisotropy on the rougher polyimide substrate. We see sharper reversal transitions and increasing coercivity on the polyimide when the Pt interlayer thicknesses are increased (Figure 4d–f), indicating increasing perpendicular magnetic anisotropy with increasing Pt interlayer thickness.[44] The increased coercivity in the transitions on Si substrates compared to the polyimide is attributed to the higher PMA on Si. For RKKY coupled magnetic bilayers on the polyimide substrate, the lower PMA due to the thin Pt insertions on either side of the Ru leads to reversals with lower coercivities, similar to the magnetic reversals seen for the single magnetic layer thin films in Figure 2g,h. Further we observe a slightly different shaped transition when going from the antiparallel state to the parallel state (toward magnetic saturation) as opposed to going from the parallel to antiparallel state (coming from magnetic saturation). The shape of these two transitions is closely linked to the population of specific types of defects which can locally increase or decrease both the magnitude of the RKKY coupling as well as the layer coercivity.[35]

We also estimate the magnitude of the RKKY coupling with an effective RKKY coupling field H_J.[43,44] While strong, the RKKY coupling on the polyimide substrate (blue and red) is reduced compared to the films grown on Si substrates (black). This is again likely due to the poorer interface quality between layers in the thin film stack owing to the high substrate roughness and defect density.[12] We further see in Figure 4g that bending the film to a R_C of 350 ± 50 µm results in no significant change in the RKKY coupling magnitude or the tunability of this coupling effect which is extremely promising for device applications on flexible substrates.

Finally, we patterned a perpendicular SAF thin film into nanowires via electron beam lithography of a resist hard mask, and subsequent Ar ion milling of the thin film stack. The nanowires were magnetically characterized using polar MOKE. In Figure 5a we see the hysteresis loop of the perpendicular SAF thin film stack on a polyimide substrate. Figure 5b,c shows the hysteresis loops of 370 and 210 nm wide and 10 µm long, straight nanowires that were patterned from the thin film and Figure 5d shows a representative array of the 210 nm nanowires with a single nanowire shown in the inset. The film is described by Ta(2)/Pt(3)/CoFeB(0.8)/Pt(0.5)/Ru(0.9)/Pt(0.5)/CoFeB(0.8)/Pt(2) with thicknesses in nm. In the thin film we observe no remanent magnetic state, and strong AF RKKY coupling as evidenced by a H_J of roughly 700 Oe. We also observe sharp, square magnetic switching processes. Similar behavior is seen in both the 370 and 210 nm wide nanowires.

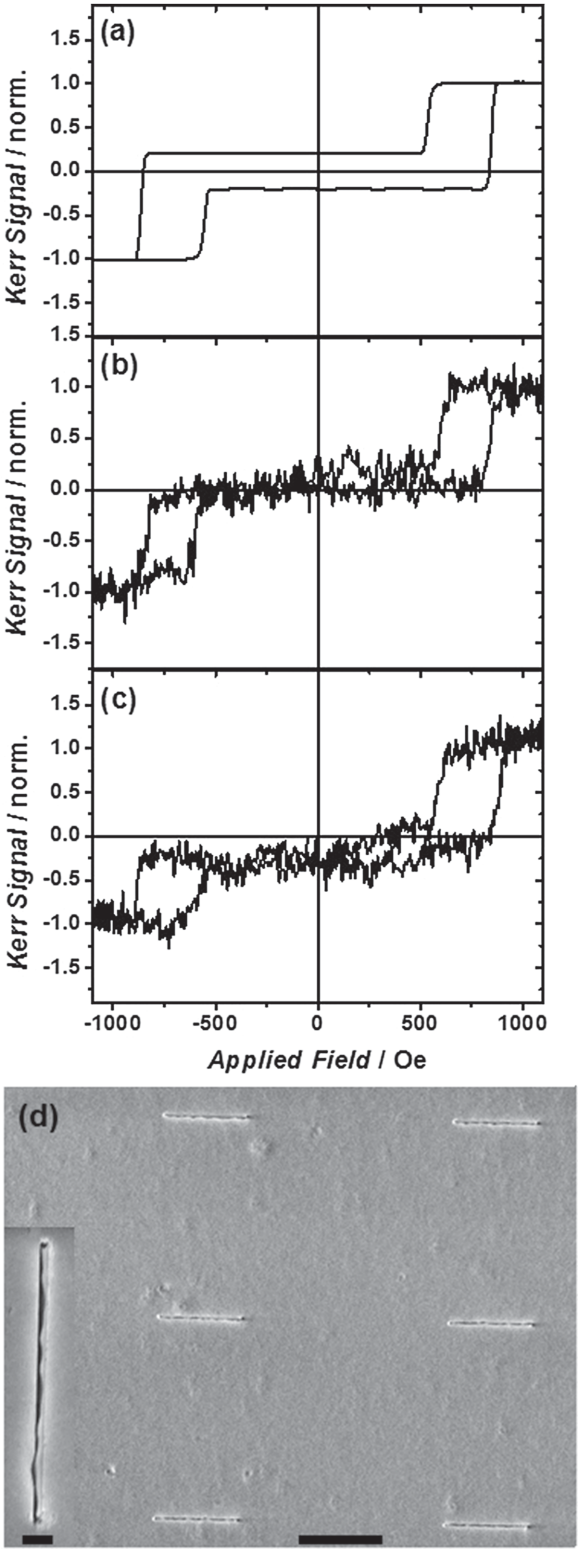

Figure 5. Polar MOKE loops taken at a field sweep rate of 4000 Oe s^{-1} on a polyimide substrate of a) a perpendicular SAF thin film, and individual nanowires of width b) 370 nm and c) 210 nm patterned from the thin film in (a). d) Scanning electron microscopy images of an array of nanowires on polyimide, each of length 10 µm, and width 210 nm (scale bar is 10 µm). The inset shows a single such nanowire (scale bar is 1 µm).

The significant increase in the noise in the signal in Figure 5b,c is expected due to the extremely low Kerr signal obtained from the switching of a single nanowire on the rough polyimide substrate. This demonstration of patterned nanoscale perpendicular SAF structures with robust magnetic characteristics is extremely promising for the fabrication of advanced spintronic devices on flexible substrates.

PMA multilayers are of great interest and technological relevance due to their high perpendicular anisotropy and tunable interfacial coupling effects which are leveraged in GMR, TMR, CIDWM, and other novel spintronic effects in devices. We demonstrate the successful fabrication of ultrathin perpendicularly magnetized CoFeB single layers on flexible polyimide substrates over a wide range of CoFeB thicknesses. The magnetic layers display high perpendicular anisotropy and sharp magnetic switching. We further successfully fabricate a SAF thin film on the flexible substrates with tunable RKKY coupling strength, and demonstrate the robust magnetic switching of AF coupled nanowires. The flexible magnetic multilayer stacks are magnetically stable even under bending to a radius of curvature of R_C of 350 ± 50 µm which is significantly lower than the expected figure of merit for most flexible electronics applications. This work opens the way for non-volatile memory, sensor, and other advanced magnetoelectronic devices based on PMA and PMA SAFs to become a part of the flexible electronics revolution.

Experimental Section

Polyimide Films: The polyimide films used were of two different types due to processing considerations. The single magnetic layers were fabricated on 25 µm thick Kapton polyimide film without an adhesive backing layer manufactured by Dupont. The SAF bilayer thin films were fabricated on 65 µm thick polyimide films manufactured by TESA with an adhesive backing layer. The adhesive backing layer allowed for ease of processing for the fabrication of the SAF nanowires during processes such as electron beam resist spinning and electron beam resist patterning.

Deposition of Magnetic Multilayers: The deposition of the magnetic thin film multilayers was done using DC magnetron sputtering. The base pressure of the sputtering system was less than 1×10^{-7} mbar. Argon was used as the sputter gas with a sputter pressure of $(7-8)\times10^{-3}$ mBar. The thicknesses of the individual layers are calibrated by growing a series of films of each material at a specific power. The thickness of each film is measured with an AFM, and a growth rate is determined from a plot of the film thickness versus the growth time. The CoFeB was sputtered at a rate of 0.05 nm s^{-1} at a power of 60 W. The various thicknesses of CoFeB were grown by adjusting the growth time. The substrates of polyimide tape and Si were introduced in to the sputter chamber simultaneously when growing the identical multilayer stack on each substrate to minimize process variation between deposition runs.

Nanowire Fabrication: The electron beam lithography resist MA-N 2403 was used as the milling mask and was spun at 6500 rpm on top of the multilayer stack grown on a polyimide substrate. The exposure was done on a CABL 9000C 50 keV e-beam system. The pattern was developed in MA-D 533 developer for 10 s. The thin film was then Ar ion milled at a milling current of 28 mA for 50 s to ensure complete removal of the surrounding film, and the milling mask was subsequently removed by dissolution in acetone followed by a brief oxygen plasma ash.

Magnetic Characterization: Polar MOKE hysteresis loops and domain imaging were collected using a NanoMOKE system from Durham Magneto Optics. Measurements for the bent samples were carried out by adhesively attaching the samples around a wire of nominal diameter 0.25 mm which was subsequently mounted in the NanoMOKE 3 system, and the curvature was measured for each sample using Vernier calipers to ensure a R_C of 350 ± 50 µm. This process was repeated for the bending measurements using metal posts for the higher diameters shown in Figure 1c.

Magnetic Figures of Merit: Effective fields are used here to characterize the perpendicular anisotropy and RKKY coupling parameters. The hard axis saturation field H_K is a measure of the magnitude of the perpendicular anisotropy and is measured via a vibrating sample magnetometry (VSM) hard axis hysteresis loop. The effective anisotropy is defined as $K_{eff} = (H_K M_S)/2$, where M_S is the saturation magnetization of the CoFeB. The interfacial or surface perpendicular anisotropy K_S is obtained from the effective anisotropy $\frac{K_S}{t_{CoFeB}} = \frac{K_{eff} + 2\pi M_S}{2}$, where t_{CoFeB} is the thickness of the CoFeB magnetic layer. Hence, we expect a decreasing $\frac{1}{t_{CoFeB}}$ dependence of the hard axis saturation field on the CoFeB layer thickness. The magnitude of the RKKY coupling is determined via a minor loop polar MOKE measurement of the SAF bilayers, where H_J is given by the shift in the minor loop caused by the SAF coupling. The magnitude of the RKKY coupling is given by $J_{RKKY} = H_J M_S t_{CoFeB}$. Further information on the characterization of the PMA and RKKY coupling may be found in the Supporting Information.

Supporting Information

Supporting Information is available from the Wiley Online Library or from the author.

Acknowledgements

This research was funded by the European Community under the Seventh Framework Program ERC Contract No. 247368: 3SPIN, the EPSRC Early Career Fellowship EP/M008517/1, a Winton Fellowship, EMRP JRP EXL04 SpinCal where the EMRP was jointly funded by the EMRP participating countries within EURAMET and the EU, and the EPSRC Cambridge NanoDTC, EP/G037221/1.

Received: November 30, 2015
Revised: February 12, 2016
Published online: May 11, 2016

[1] J. A. Rogers, T. Someya, Y. Huang, *Science* **2010**, *327*, 1603.
[2] M. C. McAlpine, H. Ahmad, D. Wang, J. R. Heath, *Nat. Mater.* **2007**, *6*, 379.
[3] G. H. Gelinck, H. E. A. Huitema, E. van Veenendaal, E. Cantatore, L. Schrijnemakers, J. B. P. H. van der Putten, T. C. T. Geuns, M. Beenhakkers, J. B. Giesbers, B.-H. Huisman, E. J. Meijer, E. M. Benito, F. J. Touwslager, A. W. Marsman, B. J. E. van Rens, D. M. de Leeuw, *Nat. Mater.* **2004**, *3*, 106.
[4] S. J. Kim, J. S. Lee, *Nano Lett.* **2010**, *10*, 2884.
[5] S. K. Hwang, I. Bae, R. H. Kim, C. Park, *Adv. Mater.* **2012**, *24*, 5910.
[6] S.-T. Han, Y. Zhou, C. Wang, L. He, W. Zhang, V. A. L. Roy, *Adv. Mater.* **2013**, *25*, 872.
[7] S. S. P. Parkin, *Appl. Phys. Lett.* **1996**, *69*, 3092.
[8] T. Uhrmann, L. Bär, T. Dimopoulos, N. Wiese, M. Rührig, A. Lechnerb, *J. Magn. Magn. Mater.* **2006**, *307*, 209.
[9] Y. F. Chen, Y. Mei, R .Kaltofen, J. I. Mönch, J. Schumann, J. Freudenberger, H. Jörg Klauß, O. G. Schmidt, *Adv. Mater.* **2008**, *20*, 3224.

[10] M. Melzer, D. Makarov, A. Calvimontes, D. Karnaushenko, S. Baunack, R. Kaltofen, Y. Mei, O. G. Schmidt. *Nano Lett.* **2011**, *11*, 2522.
[11] S. T. Purcell, M. T. Johnson, N. W. E. McGee, W. B. Zeper, W. Hoving, *J. Magn. Magn. Mater.* **1992**, *113*, 257.
[12] M. Matczak, B. Szymaski, M. Urbaniak, M. Nowicki, H. Gowiski, P. Kuwik, M. Schmidt, J. Aleksiejew, J. Dubowik, F. Stobiecki, *J. Appl. Phys.* **2013**, *114*, 093911.
[13] S. T. Purcell, W. Folkerts, M. T. Johnson, N. W. E. McGee, K. Jager, J. aan de Stegge, W. B. Zeper, W. Hoving, P. Grünberg, *Phys. Rev. Lett.* **1991**, *67*, 903.
[14] L. Thomas, G. Jan, J. Zhu, H. Liu, Y. J. Lee, S. Le, R. Y. Tong, K. Pi, Y. J. Wang, D. Shen, R. He, J. Haq, J. Teng, V. Lam, K. Huang, T. Zhong, T. Torng, P. K. Wang, *J. Appl. Phys.* **2014**, *115*, 172615.
[15] S.-W. Jung, W. Kim, T.-D. Lee, K.-J. Lee, H.-W. Lee, *Appl. Phys. Lett.* **2008**, *92*, 202508.
[16] S. Fukami, T. Suzuki, N. Ohshima, K. Nagahara, N. Ishiwata, *J. Appl. Phys.* **2008**, *103*, 07E718.
[17] I. M. Miron, K. Garello, G. Gaudin, P. J. Zermatten, M. V. Costache, S. Auffret, S. Bandiera, B. Rodmacq, A. Schuhl, P. Gambardella, *Nature* **2011**, *476*, 189.
[18] L. Liu, C. F. Pai, Y. Li, H. W. Tseng, D. C. Ralph, R. A. Buhrman, *Science* **2012**, *336*, 555.
[19] G. Yu, P. Upadhyaya, Y. Fan, J. G. Alzate, W. Jiang, K. L. Wong, S. Takei, S. A. Bender, L. T. Chang, J. Tang,Y. Jiang, M. Lang, Y. Wang, Y. Tserkovnyak, P. K. Amir, K. L. Wang, *Nat. Nano.* **2014**, *9*, 548.
[20] P. P. J. Haazen, E. Mur, J. H. Franken, R. Lavrijsen, H. J. M. Swagten, B. Koopmans, *Nat. Mater.* **2013**, *12*, 299.
[21] T. A. Moore, I. M. Miron, G. Gaudin, G. Serret, S. Auffret, B. Rodmacq, A. Schuhl, S. Pizzini, J. Vogel, M. Bonfim, *Appl. Phys. Lett.* **2008**, *93*, 262504.
[22] M. Hayashi, L. Thomas, R. Moriya, C. Rettner, S. S. P. Parkin, *Science* **2008**, *320*, 209.
[23] K.-S. Ryu, L. Thomas, S.-H. Yang, S. S. P. Parkin, *Nat. Nano.* **2013**, *8*, 527.
[24] J. L. Leal, M. H. Kryder, *J. Appl. Phys.* **1998**, *83*, 3720.
[25] S. Bandiera, R. C. Sousa, Y. Dahmane, C. Ducruet, C. Portemont, V. Baltz, S. Auffret, I. L. Prejbeanu, B. Dieny, *IEEE Magn. Lett.* **2010**, *1*, 3000204.
[26] A. Veloso, P. P. Freitas, *J. Appl. Phys.* **2000**, *87*, 5744.
[27] D. Wang, J. Brown, T. Hazelton, J. Daughton, *IEEE Trans. Mag.* **2005**, *41*, 3700.
[28] R. Lavrijsen, J.-H. Lee, A. Fernández-Pacheco, D. Petit, R. Mansell, R. P. Cowburn, *Nature* **2013**, *493*, 647.
[29] S.-H. Yang, K.-S. Ryu, S. S. P. Parkin, *Nat. Nano.* **2015**, *10*, 221.
[30] H. X. Wei, Q. H. Qin, Z. C. Wen, X. F. Han, X.-G. Zhang, *Appl. Phys. Lett.* **2009**, *94*, 172902.
[31] A. J. Baca, J.-H. Ahn, Y. Sun, M. A. Meitl, E. Menard, H.- S. Kim, W. M. Choi, D.-H. Kim, Y. Huang, J. A. Rogers, *Angew. Chem. Int. Ed.* **2008**, *47*, 5524.
[32] A. Paul, *J. Magn. Magn. Mater.* **2002**, *240*, 497.
[33] M. T. Johnson, P. J. H. Bloemen, F. J. A. den Broeder, J. J. deVries, *Rep. Prog. Phys.* **1996**, *59*, 1409.
[34] D. Chiba, M. Kawaguchi, S. Fukami, N. Ishiwata, K. Shimamura, K. Kobayashi, T. Ono, *Nat. Commun.* **2012**, *3*, 888.
[35] J. H. Lee, R. Mansell, D. Petit, A. Fernández-Pacheco, R. Lavrijsen, R. P. Cowburn, *SPIN* **2013**, *3*, 4.
[36] R. Ploessl, J. N. Chapman, M. R. Scheinfein, J. L. Blue, M. Mansuripur, H. Hoffmann, *J. Appl. Phys.* **1993**, *74*, 7431.
[37] Y. C. Hsieh, M. Mansuripur. *J. Appl. Phys.* **1995**, *78*, 380.
[38] M. T. Rahman, N. N. Shams, Y.-C. Wu, C.-H. Lai, D. Suess, *Appl. Phys. Lett.* **2007**, *91*, 132505.
[39] J. H. Franken, M. Hoeijmakers, R. Lavrijsen, H. J. M. Swagten, *J. Phys.: Condens. Matter* **2012**, *24*, 024216.
[40] N.-H Kim, D.-S. Han, J. Jung, J. Cho, J.-S. Kim, H. J. M. Swagten, C.-Y. You, *Appl. Phys. Lett.* **2015**, *107*, 142408
[41] S. Emori, U. Bauer, S.-M. Ahn, E. Martinez, G. S. D. Beach, *Nat. Mater.* **2013**, *12*, 611,
[42] P. Bruno, C. Chappert, *Phys. Rev. B* **1992**, *46*, 261.
[43] R. Lavrijsen, A. Fernández-Pacheco, D. Petit, R. Mansell, J. H. Lee, R. P. Cowburn, *Appl. Phys. Lett.* **2012**, *100*, 052411.
[44] S. Bandiera, R. C. Sousa, S. Auffret, B. Rodmacq, B. Dieny, *Appl. Phys. Lett.* **2012**, *101*, 072410.

